Applied Thermal Engineering 73 (2014) 1041–1054

Contents lists available at ScienceDirect

Applied Thermal Engineering

journal homepage: www.elsevier.com/locate/apthermeng

Dynamic model based on experimental investigations of a wood pellet steam engine micro CHP for building energy simulation

Jean-Baptiste Bouvenot [a, *], Benjamin Latour [a], Monica Siroux [a], Bernard Flament [a], Pascal Stabat [b], Dominique Marchio [b]

[a] ICube UMR7357, Université de Strasbourg, INSA Strasbourg, 24 boulevard de la Victoire, 67 084 Strasbourg Cedex, France
[b] Mines Paristech, Centre d'efficacité énergétique des systèmes, 60, Boulevard Saint Michel, F 75 272 Paris Cedex 06, France

HIGHLIGHTS

- A wood pellet steam engine micro CHP device has been tested.
- A micro CHP data driven dynamic model has been implemented in TRNSYS environment.
- The model takes into account transient and steady state phases.
- The model is suitable with building energy simulation.

ARTICLE INFO

Article history:
Received 16 May 2014
Accepted 31 August 2014
Available online 6 September 2014

Keywords:
Micro CHP
Wood pellet
Steam engine
Dynamic model
Experimental

ABSTRACT

A wood pellet micro combined heat and power device (μCHP) has been tested in order to characterize its performances in steady and transient states. A dynamic model based on these experimental investigations has been developed in order to predict its energy performances and its pollutant emissions. The model is designed with a few parameters experimentally accessible. This model has been implemented in TRNSYS numerical environment. This work focuses on the experimental investigations and on the model description. The modelling approach is based on a physical part (an energy balance on the entire device and a combustion model), and on an empirical part (correlations for the fuel power input and for the thermal and electrical outputs). The model characterizes the μCHP behaviour for different part load ratios (PLR) (power modulation). The dynamic phases with start-up and cooling phases are also taken into account.

1. Introduction

Micro combined heat and power (μCHP) is an emerging means in order to produce simultaneously heat and power with high efficiency. CHP (or cogeneration) valorises the residual heat generated during power production by means of thermodynamic cycles such as Rankine or Stirling cycles. This heat production is used for space heating and domestic hot water (DHW) while the electricity production can be used in building or exported on the grid compared to centralized power plants such as nuclear, gas or coal power plants that use cooling towers to remove the heat. CHP power plants increase the energetic efficiency and decrease the environmental impacts by consuming less primary energy [1–3].

CHP is already widespread in industrial applications or building applications in district heating for a power range of MW in order to be suitable for electrical and heating needs. μCHP corresponds to power compatible with residential or commercial heating and power needs. μCHP systems have a power output below 20 kW_{el} [4]. The technologies which are used are different from centralized power plants [5] and the electrical efficiencies are lower. These decentralized systems also reduce losses on distribution networks [6]. The main conversion processes which are used for μCHP applications are: internal combustion engines (ICE), micro turbines, Stirling engines, Ericsson engines, steam engines (SE) and fuel cells [1], [7]. Steam engines present certain advantages compared to the other technologies. The systems are simple by using free pistons or rotary engines, their design is cheap and the steam is easy to generate with any fuels such as gas, oil, solar energy or biomass [8]. At micro scale, the use of the Rankine cycle thresholds power efficiency at about 10% but heat recovery can be very high [8]. Dong

* Corresponding author. +33 388144967.
E-mail address: jean-baptiste.bouvenot@insa-strasbourg.fr (J.-B. Bouvenot).

http://dx.doi.org/10.1016/j.applthermaleng.2014.08.073
1359-4311/

et al. [9] made a review of all technologies suitable with biomass μCHP applications. They conclude that the biomass fuel can be applied to all classical μCHP technologies listed before and they describe all the energy conversion processes of the biomass: combustion for steam generation, gasification, pyrolysis or biochemical processes.

A power modulating wood pellet steam engine μCHP (WP SE μCHP) device has been tested to characterize its behaviour in steady and transient states. The objective of this paper is to describe the experimental characterization of a WP SE μCHP leading to a performance based model dedicated to annual building simulations.

The behaviour and the performances of μCHP systems are still little known; in particular WP μCHP devices are little studied [10]. Among the existing commercial μCHP devices, only some of them use renewable fuels. Table 1 sums up the existing devices on the market or under development.

Some works have been achieved on biomass μCHP devices. Thiers et al. [10] propose a study on a commercial WP μCHP device using a Stirling engine (Sunmachine). Thermal and electrical outputs have been studied. Some works propose to couple a classical boiler (using gas, fuel or biomass) with an organic Rankine cycle (ORC). Cardozo et al. [11] connected an overfed WP burner to a gamma type Stirling engine. This configuration led to an overall efficiency of 77% and an electrical efficiency of 9%. Guoquan et al. [12] underline the relevance to connect a biomass boiler used as steam generator to a steam engine. They carried out a prototype which links an ORC engine with a biomass boiler but the electrical efficiency only reaches 1.48%. Cordiner et al. [13] used a compressor as steam expander connected to a biomass furnace. Experimental studies led to an electrical efficiency of 13% with an electrical output of 70 kW. Alanne et al. [14] studied the implementation of a thermoelectric cogeneration system inside a biomass boiler. Theoretically, electrical efficiencies of 9% can be reached. They also studied the coupling between a rotary steam engine and a biomass boiler where electrical efficiencies can also theoretically reach 9% [8]. Creyx et al. [15] studied the opportunity to couple a hot air engine based on an Ericsson cycle with a biomass boiler where theoretical thermodynamic efficiencies of about 37.6% can be reached. Prando and al [16] propose to couple a biomass gasification reactor to an internal combustion engine for residential applications. Finally, Angrisani and al [17] developed a concept of solar-biomass μCHP system based on a fluidized bed and a Stirling engine designed to produce about 1 kW_{el}.

Table 1
Review of commercial WP (or which accepts any fuel) μCHP devices.

Manufacturer	Apparatus	Power		LHV efficiency	
		Electric [kW_{el}]	Thermal [kW_{th}]	Electric [%]	Thermal [%]
Stirling engine					
● ÖkoFEN	Pellematic Smart_e	1.1	15.8	7	95
● Sunmachine	Pellet	1.5–3	4.5–10.5	20–25	65–70
Rankine: scroll turbine (module to connect to external heating source)					
● Enerftech	EnefcogenPLUS	5	33	12.5	82.5
● Eneftech	Enefcogen GREEN	5–10	45–80	10.5	84.2
Rankine: scroll turbine					
● Novotek industry	COGEMAX 14	0.6–1.5	4.8–12	10	82
Rankine: steam engine (linear free piston)					
● Exoes/Otag	BISON	0.3–1.6	3–16	9	83
Rankine: steam engine (module to connect to external heating source)					
● Exoes	SHAPE	3	50	6	84

● ready.
● introducing phase.
● testing and optimization phase.

Different modelling approaches exist to simulate the behaviour of a μCHP device. A full physical model requires the modelling of the combustion reaction, the thermodynamic cycle and mechanical and electrical conversion with non-ideal efficiencies. This approach needs data on the engine and the model supposes low computing time steps which are not suitable with annual dynamic building energy simulations. The usual time steps for accurate thermodynamic models (from the order of 10^{-3} to 10^{-6} s) are very different in comparison to buildings (from 1 min to 1 h). Moreover, to correctly model an engine, many features have to be known like heat exchanger surfaces, work pressures, geometry, etc, which are generally unknown. Alanne et al. [8] implemented a thermodynamic model of a rotary steam engine using a Rankine cycle by taking into account work pressures, isentropic efficiency or expansion volumes. Creyx et al. [15] developed a thermodynamic model on expansion and compression phases of an Ericsson engine coupled to a biomass boiler for design optimization applications on the operating pressures and temperatures. This model is not used for energy building simulations. Lontsi et al. [18] developed a thermodynamic model of a Joule cycle reciprocating Ericsson engine for μCHP systems which takes into account start-up phases. This system would be suitable with renewable fuels such as biomass fuel. The simulation time step is 2.10^{-3} s, and the model is used to optimize the design of the engine.

Semi-physical simplified models of internal combustion engine and Stirling engine have been developed for annual energy building simulation. In the International Energy Agency (IEA)/Energy Conservation in Buildings and Community Systems (ECBCS) Annex 42, Beausoleil-Morrison et al. [19] propose a general physical and parametric model without thermodynamic considerations which is suitable with biomass applications. The Annex 42 gives a literature review on models of mini-and μCHP tools for dynamic simulation of buildings. The Annex 42 proposes a method to model μCHP distinguishing steady states and transient phases through grey box models. It distinguishes 4 phases: stand-by, warm-up, steady state and cool down phases. These models use thermal inertia to model transient phases. Steady state performances are calculated by using correlations based on the main parameters that influence thermal and power inputs and outputs: the cooling water temperature and mass flow. The required time step is suitable for annual dynamic thermal simulation (a few minutes). Lombardi et al. [20] have simplified this model by implementing a linear difference model based on linear coefficients and reference parameters which are determined by a few experimental tests.

Furthermore, “black box” models have been developed. Thiers et al. [10] propose a simple model on a WP SE μCHP by using a fully empirical modelling approaches based on experimental investigations. They have fitted a quasi-static model from a measurement campaign conducted on the Sunmachine. The preheating and cooling phases are characterized only on the

combustion chamber temperature. This model is strictly limited to the tested product and to the achieved test conditions (source temperatures, water flow rates, fuel characteristics, heating loads). The thermal and electrical outputs are calculated only in steady states according to the inlet cooling water temperature.

Indeed, Conroy et al. [21] made a data driven numerical model of a Stirling engine μCHP device based on field tests. The accuracy of the measurements is not given and the fitting only depends on time without physical meaning.

Our objective is to build a simple and accurate dynamic model which requires the fewest parameters. These parameters have to be easily reachable by experimental investigations or manufacturer data in order to carry out optimization simulations on annual energy building simulations at low simulation time steps (up to 1 min). The parametric model developed in the Annex 42 is the closest to these objectives.

Many studies are carried out in order to assess the primary energy gains or the environment impact of μCHP without taking into account the transient behaviour of the μCHP devices and by only using constant heat to power ratio or constant efficiencies [1,6,22,23]. Hawkes et al. [24] investigated the influence of the simulation time step of the electrical and thermal demands on the energetic, economic and environmental performances of μCHP integrated to buildings. They conclude that the results are very sensitive to the time step when varying between 1 h and 5 min: low temporal resolution lead to μCHP oversizing, economic gains underestimations and environmental impact overestimations. Only a power ramp rate, the minimum/maximum power output and the efficiencies in steady state are used for the μCHP model. The transient behaviour of the μCHP devices is not taken into account. The objective of the developed model is to consider the dynamic behaviour of the μCHP in order to assess the performances of μCHP integrated in residential buildings.

This paper focuses on the test bench description, on the experimental investigations and results of a WP μCHP using a linear free piston steam engine and on the model description.

2. Experimental study

2.1. Description of the wood pellet μCHP test bench

The experiments have been carried out on the WP μCHP BISON from EXOES. The WP μCHP unit has a steam engine (linear free piston) supplied by a steam generator which can produce steam up to 20 bars and 400 °C. According to the manufacturer, the thermal output can vary from 3 to 16 kW_{th} and the electrical output can vary from 0.3 to 1.6 kW_{el}. The device controls the incoming combustion air flow to vary the load. The supply of pellets is controlled to maintain a constant level of pellet inside the combustion chamber. The pellet supplier is indirectly controlled by the device to control the part load ratio (PLR). The test bench has been designed in order to study instantaneous heating or full heat storage configurations as is shown in Fig. 1. For the heat storage configuration, the PLR is controlled according to the tank top temperature. For the experimental tests, the volume flow rate and the PLR are fixed and the inlet water temperature is controlled according to the set point by playing on a 2 ways valve on the heating circuit.

The electrical power output and electrical auxiliary consumption (starter, pumps, fan, WP feeder, air compressor, and ash extractor) are measured by two separate watt meters. Thermal output is assessed by using a flow meter and two temperature probes. A gas analyser is used to perform measurements on the exhaust gas. The fuel mass flow is assessed by using a scale on which the storage tank is placed. The WP feeder is mounted on a support in order to avoid pressing on the WP storage tank. The connection between the feeder and the WP storage tank has been designed in order to avoid any contact.

The μCHP unit is composed of 4 levels (Fig. 2). The first one at the top is composed of the steam generator where combustion occurs. There is also an air compressor and a high pressure bottle in order to clean up the pipes of the heat exchanger (steam generator) each 1000 s. The second one in the middle is composed of the steam engine which is supplied by steam coming from thin highly isolated pipes. Under the combustion chamber, there is a starter which heats up the WP inside the combustion chamber to launch the combustion. The third one is composed of the tank which receives the hot condensates from the steam engine. There is also a high pressure pump (HP pump) which is used during the start-up and cooling down phases. It pumps the low pressure water from the heat exchanger to supply the steam generator at high pressure. Hot condensates from overheated steam are stored in the tank before being pumped up to the heat exchanger which is on the last level at the bottom. There are also 3 pumps: one for the primary heat circuit, one for the heat distribution circuit in the building and one which is a vacuum pump to control the low pressure level in the tank.

2.2. Metrology

Table 2 summarizes all the metrological means implemented on the test bench. The global uncertainties for each quantity are calculated according to the law of propagation of uncertainty [25–28].

2.2.1. Fuel power

The fuel power which is supplied to the device is calculated by Eq. (1) based on the fuel mass flow and on the LHV which is derived from laboratory tests on WP samples.

$$P_{fuel} = \dot{m}_{fuel} LHV \quad (1)$$

The fuel mass flow is calculated with a scale which has been chosen in order to minimize the uncertainty. Since the greater the

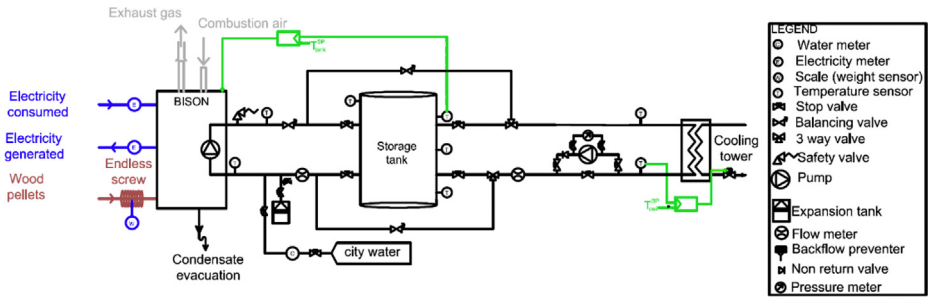

Fig. 1. Operating scheme of the test bench (with the control strategy principle on the tank and inlet temperatures).

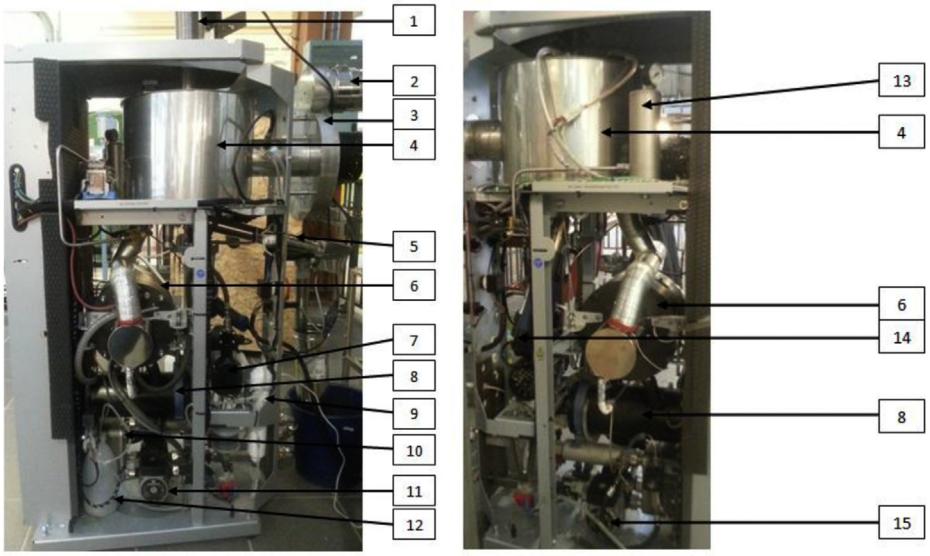

Fig. 2. Technical description of the BISON (1: WP supplier, 2: exhaust gas, 3: fan, 4: steam generator, 5: ash extractor, 6: linear generator, 7: high pressure pump, 8: tank, 9: filter, 10: heat exchanger, 11: primary circuit pump, 12: buffer tank, 13: compressed air tank, 14: starter, 15: secondary circuit pump).

Table 2
Metrological means and associated uncertainties.

Type	Parameter	Notation	Metrologic means	Uncertainty
Fuel input	Consumed fuel	m_{fuel}	Scale (Mettler Toledo ICS425)	±10 g
	LHV	LHV	DIN EN 14,774–2	±0.1 kWh/kg
	Fuel and air temperature	T_{amb},T_{fuel}	4 wires Pt100	±0.2 K + 0.05%
	Fuel power	P_{fuel}	Calculated Eq. (2)	±3%
Heating output	Water temperature	$T_{cw,i}$, $T_{cw,o}$	4 wires Pt100	±0.2 K + 0.05%
	Volume flow	$\dot{V}_{cw}$	Blade flow meter (Bürkert M12)	±0.15 lL/mn + 2.5%
	Thermal power	$\dot{Q}_{HX}$	Calculated Eq. (1)	±4.5 to 7.3 % (according to PLR)
Electric output	Gross electric power	P_{gross}	Energymeter (Socomec DIRIS A20)	1%
Electric input	Consumed power	P_{aux}	Energymeter (Socomec DIRIS A20)	1%
Tank temperature	Storage tank temperature	T_{tank} (x4)	4 wires Pt100	±0.2 K + 0.05%
Exhaust gas	Temperature		Analyser ECOM J2KN	–
	O_2, NO_x, CO, CO_2			–

weight range is, the greater is the measurement uncertainty, a compromise has been found in order to threshold the WP storage tank capacity to a 8 h full load test. The mass flow is smoothed on the whole test so as to avoid noise on the measurements linked to the feeder vibrations in the WP mass and WP dynamic movements inside the tank (Fig. 3). The mass flow corresponds to the slope of the mass variation. The uncertainty is mastered by choosing the test time according to the PLR in order to reach an uncertainty below 1% (Table 2).

2.2.2. Thermal power

Thermal power is calculated by using the current equation of heat transport (Eq. (2)).

$$\dot{Q}_{HX} = \rho(T_{cw,i}) \cdot \dot{V}_{cw} \cdot (c_{cw}(T_{cw,o}) \cdot T_{cw,o} - c_{cw}(T_{cw,i}) \cdot T_{cw,i}) \quad (2)$$

The variations of the thermal properties with the temperature of the heating water are taken from Holman [29]. The density is calculated with the cooling water inlet temperature because the flow meter is located on the backflow, just before the temperature probe. The thermal efficiency is given by Eq. (3):

$$\eta_{th} = \frac{\dot{Q}_{HX}}{P_{fuel}} \quad (3)$$

2.2.3. Electrical power

The electrical power is recorded by 2 W m, one measuring the incoming electricity for the operation of the auxiliary devices and the other measuring the gross electricity which is produced by the

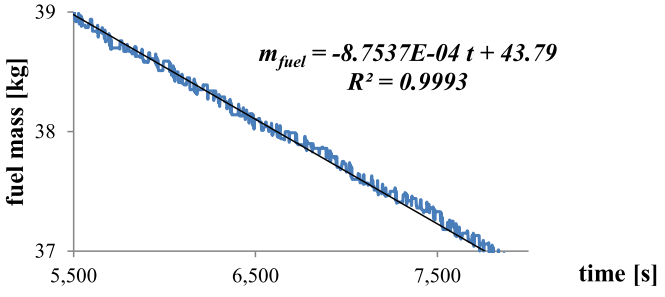

Fig. 3. WP mass variation measurements for PLR = 80%.

steam engine. The uncertainty is below 1% (Table 2). The gross electrical efficiency is given by Eq. (4):

$$\eta_{el} = \frac{P_{gross}}{P_{fuel}} \tag{4}$$

We also define the power to heat ratio and the global efficiency by Eqs. (5) and (6):

$$\sigma = \frac{P_{gross}}{\dot{Q}_{HX}} \tag{5}$$

$$\eta_g = \eta_{th} + \eta_{el} \tag{6}$$

3. Experimental results

The experimental investigations aim at assessing accurate energy performances of the device and well characterize the transient phases: the start-up and the cooling phases.

3.1. Steady state phases

Experimental tests have been made on a PLR range of [22 %–98%] by step of about 10%, on a water inlet temperature range of [30 °C–45 °C] by step of 5 °C and on a water volume flow rate range of [5 L/min–15 L/min] with a step of 5 L/min. Tests made from 40% to 80% of PLR show the low influence of the water inlet temperatures and the flow rates on the thermal, electrical and fuel power (Figs. 4 and 5). The influence of these parameters is lower than the uncertainty or repeatability ranges of the measurements. The thermal efficiency is not impacted by the variation of the water flow rate of the heating circuit. Heat recovery and steam generation are separated.

The variation range of the cold source temperature is very low (maximum gap of 15 °C) compared to the difference between the hot source (inside the combustion chamber up to about 900 °C) and the cold source (condensate steam in the tank) that makes an insignificant influence on the thermal and electrical performances. This device does not take profit of the exhaust gas condensation so the performances are low dependent on these 2 parameters. For any cooling water flow rate or temperature, the steam is produced by playing on the incoming combustion air and WP feeder. This steam is injected into the engine to produce power. Then, the steam is condensed in the buffer tank. The temperature of the buffer tank

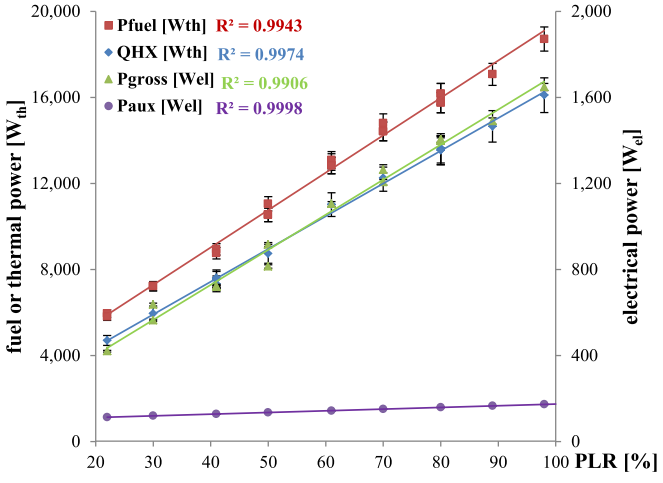

Fig. 4. Steady state results on fuel, thermal and electrical powers.

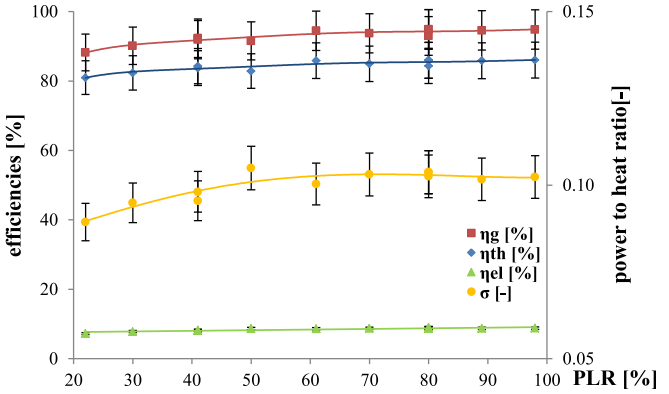

Fig. 5. Steady state results on the global, thermal and electrical efficiencies and on the power to heat ratio.

depends on the withdrawal of heat toward the heating circuit. There is no correlation between the temperature level in the tank and the physical properties (pressure and temperature) of the steam injected into the engine (which is controlled). During the tests, the volume flow and inlet cooling water temperature have been chosen to minimize the uncertainty range. The thermal, fuel, electrical and auxiliary powers are linear according to the PLR which is an internal parameter of the device (Fig. 4). These 4 quantities do not tend toward 0 when the PLR tends to 0, so the validity range of the PLR for the linear correlations is only between 22 and 98%.

The efficiencies are highest for full load operations and the global efficiency can reach 95% on LHV (Fig. 5). The efficiencies decrease slightly with the PLR reduction up to 22%. The power to heat ratio is relatively stable around 0.1 up to 41% of PLR. This device has similar energy performances to others existing or developing biomass Rankine μCHP devices (Table 1).

Experimental investigations also show other main results that are useful for the numerical model such as the oxygen rate in the wet flue gas which is controlled at a constant value of 6.2% or the ash temperature at the bottom of the combustion chamber which is constant for any PLR at about 230 °C.

The exhaust gas has also been studied. The CO and NO contents have been measured using a gas analyser (J2KN from ECOM) as well as the temperature during 2 h long tests. Fig. 6 gives the mean values of the CO and the NO volumetric contents according to the PLR. The NO production increases with the PLR although CO emissions are almost constant according to the PLR ranging between 20 and 40 ppm. These values are very lower than values fixed by the European standard on wood pellet boilers (EN 12809). The NO emissions increase with the exhaust gas temperature which is linked to the PLR. The exhaust gas temperature will let to calculate the exhaust gas heat losses. As it has been noticed in Fig. 4, the exhaust gas temperature and the CO and NO volumetric contents do not tend toward 0 when the PLR tends to 0. The linear correlations for these quantities are again valid only for a PLR range between 22 and 98% which are the minimum and maximum PLR of the tested device.

3.2. Start-up phase

The μCHP device at the beginning uses the 2 pumps of the secondary and primary circuits, the fan and the electronic card. Then, after 20 s on average, the starter begins to warm up the combustion chamber with a mean electrical power of 1250 W for an average time of 300 s. The thermal production begins on average

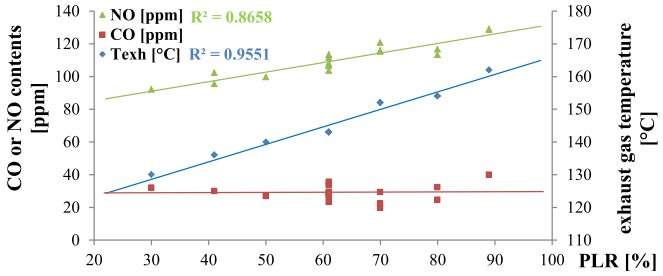

Fig. 6. Steady state CO and NO contents in exhaust gas.

after 450 s, the engine is bypassed and the steam supplies directly a coaxial heat exchanger on the heating circuit. The PLR set point is constant at 27% for each start-up phase. Then, the high pressure pump is triggered until the steam engine starts after 670 s on average. Fig. 7 gives the behaviour of each quantity during the start-up phase. The engine is used in steady state operation to pump water from the low pressure to the high pressure circuits by using a part of the mechanical energy of the engine. On average, the start-up cycle involves additional 142 Wh_{el} of electrical energy which is consumed by the start-up devices (starter, over use of the WP feeder and the high pressure pump) before launching the electrical production. In Fig. 7, the abrupt loss of thermal power after 700 s comes from the switch in the hydraulic circuit and the beginning of the conversion of a part of the heat in power. The total duration start-up cycle is on average of 1100 s to reach the steady state values of each quantity. Indeed, as soon as the starting cycle of the engine is triggered, the overheated steam is injected in the main cold circuit, that is why the system needs time to extract the heat from the system because the condensates tank need to be thermally loaded. The trend curves in Fig. 7 will be used to model the start-up phases.

The fuel mass flow rate variation is also measured. There is an ignition in order to supply the combustion chamber by about 100 g of biomass fuel. Then, as soon as the starter turns off, the combustion starts and the feeder works for about 150 s in order to completely fill the combustion chamber with about 500 g of biomass fuel (Fig. 7 between 350 and 500 s). Then, the mass variation is linear during steady state (Fig. 3) and the variation only depends on the PLR. The WP feeder operates according to the PLR to fulfil the combustion chamber in order to maintain the WP level as constant thanks to a light sensor. The higher the PLR is, the greater is the electrical consumption of the feeder. This increasing is integrated in the whole electrical consumption of the auxiliary devices (Fig. 4).

3.3. Cooling phase

During the cooling phase, any fuel is consumed and the thermal and electrical power decrease (Fig. 8). Electrical production decreases up to a threshold of 500 W. The thermal production keeps

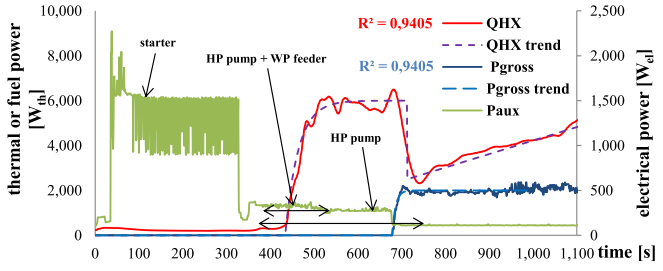

Fig. 7. Start-up phase: electrical consumption, electrical and heating productions for PLR = 27%.

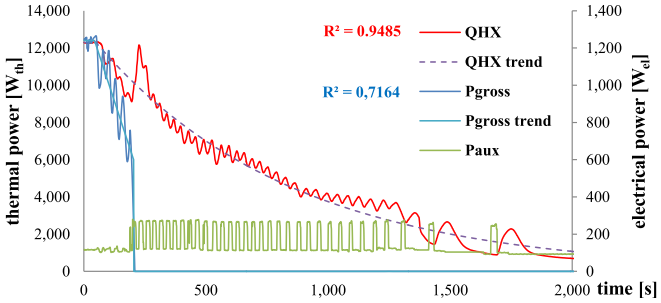

Fig. 8. Cooling phase: thermal and electrical production and auxiliary consumption for PLR = 80%.

occurring until the end of the combustion of the remaining biomass fuel. As soon as the engine is switched off, the high pressure pump is turned on intermittently during the whole of the cooling phase. The cooling phase ends when the high pressure pump stops, after 1800 s on average. The auxiliary electrical overconsumption linked to this pump reaches on average 38 Wh_{el}. The trend curves in Fig. 8 will be used to model the cooling phase.

3.4. Modulating phase

When the PLR varies, the device has a response time. There is a power ramp rate which cannot be exceeded to reach the PLR set point. Tests have been carried out to assess this speed which reaches 6 W_{th}/s for the thermal power and 0.6 W_{el}/s for the electrical production (Fig. 9).

3.5. Exhaust gas

The start-up and the cooling phases have been studied in order to assess the pollutant emissions which are higher during these 2 phases. NO emissions are stable during the start-up phase although CO emissions are higher than steady state emissions (Fig. 10). During the cooling phase, both the CO and NO emissions are higher than steady state emissions. During the start-up phase, the CO emissions are higher because at the beginning, the combustion chamber is cold and the low temperatures slow down the oxidation of the biomass carbon and generates more CO [30]. During the cooling phase, an oversupply of air occurs that also cools down the combustion chamber. The NO emissions remain stable for each phase.

3.6. Ash production

The ash content has been assessed by recovering the ash during long tests (at least 24 h) in order to increase the accuracy. An ash content in the WP of 0.3% has been found on average.

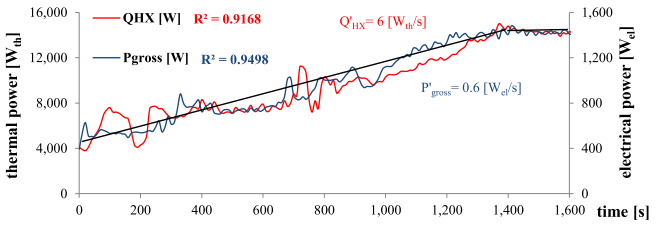

Fig. 9. PLR variation speed in response of a PLR step change from 27 to 90%.

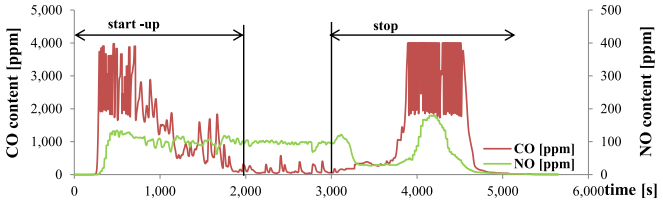

Fig. 10. CO and NO emissions during the transient phases.

4. Wood pellet micro CHP numerical model

The developed model is mainly based on the previous experimental studies. The 4 phases described in the Annex 42 are studied separately. 3 parameters have been studied: the PLR, the cooling water mass flow and the inlet water temperature. The experimental results show that only the PLR plays on the performances. The main reason is that the studied device does not recover the latent heat from the condensation of the steam inside the exhaust gas.

A model has been developed in the TRNSYS environment under the name of Type 254 in order to well characterize the physical behaviour of the μCHP. The model tries to match the objectives of simplicity and accuracy to be suitable with annual dynamic thermal building simulations this is the reason why it is designed as a grey box model with a physical part and an empirical part. The energy balance and the combustion model are physical and the main inputs and outputs are calculated by using correlations according to the PLR coefficient. In steady state, the energy balance has to be respected:

$$\dot{H}_{fuel} + \dot{H}_{air} + P_{fuel} = P_{gross} + \dot{Q}_{loss} + \dot{Q}_{HX} + \dot{H}_{exh} \quad (7)$$

In steady state conditions, the electricity power, the fuel mass flow and the heating power are assessed by correlations dependent on the PLR by using the linear differences model of Lombardi [20]. The combustion model is based on classical chemical reactions involving the combustion air, the fuel and the reaction products.

4.1. Steady state phase

The expressions of the delivered thermal output, fuel input, and gross electric power (in W), are defined as a function of the nominal conditions for each value with $PLR_{nom} = 100\%$ ($PLR \in [22 - 100]$) by Eqs. (8)–(10) (LHV is given in kWh/kg_{fuel})

$$P_{fuel} = 1000 \cdot \left(a(PLR - PLR_{nom}) + \dot{m}_{fuel}^{nom}\right) LHV \quad (8)$$

$$\dot{Q}_{HX} = b(PLR - PLR_{nom}) + \dot{Q}_{HX}^{nom} \quad (9)$$

$$P_{gross} = c(PLR - PLR_{nom}) + P_{gross}^{nom} \quad (10)$$

The net electrical power corresponds to the usable part of electricity produced by the engine. The other part of the production is self-consumed by the auxiliaries (pumps, fans, electronic card, etc.). The net electrical power is defined by Eq. (11).

$$P_{net} = P_{gross} - P_{aux} \quad (11)$$

$$P_{aux} = d(PLR - PLR_{nom}) + P_{aux}^{nom} \quad (12)$$

For the model identification, the LHV of the fuel should be known or measured. The outlet cooling water temperature is calculated using the heat transport equation:

$$T_{cw,o} = \frac{\dot{Q}_{HX}}{c_{cw}\dot{m}_{cw}} + T_{cw,i} \quad (13)$$

The Appendixes 1 and 2 present the transient states transition conditions and the algorithm chart with the main inputs and outputs with internal calculations.

4.2. Transient phases

In addition to the steady state characterization, the start-up and cooling transient phases need to be modelled. These phases are modelled by exponential laws and delay times (Figs. 7 and 8). The modification of the PLR set point is not instantaneous in reality. In the numerical model a power ramp rate is implemented (Fig. 9). If a PLR set point occurs, the process value of PLR will vary according to the power ramp rate. For the electrical consumption of the auxiliaries, the overconsumption of the electrical energy linked to these devices for each phase is divided by the transient phase duration: 670 s for the start-up phase and 1800 s for the cooling phase (Eq. (14) and (15)).

$$\text{if } t < t_{start} + \Delta t_{start}^{P} \quad P_{aux}^{start} = P_{aux}(PLR_{start}) + \frac{E_{start}^{P}}{\Delta t_{start}^{P}} \quad (14)$$

$$\text{if } t > t_{stop} + \Delta t_{stop}^{P} \quad P_{aux}^{stop} = P_{aux}(PLR_{stop}) + \frac{E_{stop}^{P}}{\Delta t_{stop}^{Q} - \Delta t_{stop}^{P}} \quad (15)$$

The Appendix 3 presents the modelling representation of the start-up and the cooling phases.

4.3. Combustion modelling

From the fuel mass flow rate, the fuel composition and the combustion air excess, typical combustion calculations are undertaken in order to assess the CO_2 mass flow rate and exhaust gas heat losses.

4.3.1. Chemical composition and energy density of the wood pellet

The model requires the mass fraction of each of the following elements on dry fuel: oxygen (O), carbon (C), hydrogen (H), the ash content and the water content. Either the chemical composition is derived from laboratory tests as has been carried out here (Table 3), or default values are proposed: the chemical composition of the pellet is quite stable and the default values can be used with a good accuracy [31,32]. For the ash content, laboratory tests can be carried out or the standards [32] or the manufacturer data can be used.

The LHV and the water content in the fuel are two key values of the model. Either they are also derived from laboratory tests or default values are proposed. Bernard [30] proposes a simple formula based on the mass composition of the dry WP and which gives the LHV value of the dry part of the WP (Eq. (16)). The LHV on the dry part takes into account the required energy for the transformation of the hydrogen in the WP and which is turned into water.

Table 3
Experimental and theoretical WP characterization.

	w [%]	Y_{ash} [%]	$Y_{C\ dry}$ [%]	$Y_{H\ dry}$ [%]	$Y_{O\ dry}$ [%]	LHV_{dry} [kWh kg^{-1}]	LHV [kWh kg^{-1}]
Experimental	6.6	0.34	51.3	6.2	42	5.29	4.9
Theoretical	8	0.4	50	6	44	5.34	4.9

$$\mathrm{LHV} = (1-w)\left(34,030\,Y_{C\ \mathrm{dry}} + 121,640\,Y_{H\ \mathrm{dry}} - 12,540\,Y_{O\ \mathrm{dry}}\right) - w\,L_v \tag{16}$$

Here, the LHV, the chemical composition and the water content have been tested in a laboratory by using specific test standards (Table 2).

4.3.2. Wood pellet combustion reactions model

The chemical reaction of the dry part of the input fuel mass flow rate, without the ash part which is neglected, gives:

$$C_xH_yO_{z(s)} + \left(x+\frac{y}{4}-\frac{z}{2}\right)\left(1+e_{\mathrm{air}}\right)O_{2(g)} \rightarrow xCO_{2(g)} + \frac{y}{2}H_2O_{(g)} + \left(x+\frac{y}{4}-\frac{z}{2}\right)e_{\mathrm{air}}O_{2(g)} \tag{17}$$

Different values are calculated in order to know each mass flow rate of each component.

$$\dot{m}_{\mathrm{fuel}} = \frac{P_{\mathrm{fuel}}}{\mathrm{LHV}} \tag{18}$$

$$\dot{m}_{\mathrm{air}} = \dot{m}_{\mathrm{fuel}}(1-w)\frac{x+\frac{y}{4}-\frac{z}{2}}{M_{C_xH_yO_z}}(1+e_{\mathrm{air}})\frac{\left(\chi_{O_2}M_{O_2}+\chi_{N_2}M_{N_2}\right)}{\chi_{O_2}} \tag{19}$$

The content of water in exhaust gas is composed from 2 contributions: the part which comes from the hydrogen content of the dry WP and the part which comes from the water content of the wet WP.

$$\dot{m}_{H_2O} = \dot{m}_{\mathrm{fuel}}\left(w + (1-w)\frac{y}{2}\frac{M_{H_2O}}{M_{C_xH_yO_z}}\right) \tag{20}$$

CO_2, N_2 and O_2 mass flows in exhaust gas are calculated by using following Eqs. (21)–(23):

$$\dot{m}_{CO_2} = \dot{m}_{\mathrm{fuel}}(1-w)\frac{xM_{CO_2}}{M_{C_xH_yO_z}} \tag{21}$$

$$\dot{m}_{N_2} = \dot{m}_{\mathrm{fuel}}(1+e_{\mathrm{air}})(1-w)\left(x+\frac{y}{4}-\frac{z}{2}\right)\frac{\chi_{N_2}}{\chi_{O_2}}\frac{M_{N_2}}{M_{C_xH_yO_z}} \tag{22}$$

$$\dot{m}_{O_2} = \dot{m}_{\mathrm{fuel}}e_{\mathrm{air}}(1-w)\left(x+\frac{y}{4}-\frac{z}{2}\right)\frac{M_{O_2}}{M_{C_xH_yO_z}} \tag{23}$$

The combustion air excess which is required to ensure a good quality of combustion is often unknown. To reach this parameter, Eq. (24) gives the link between this air excess and the oxygen rate in the wet exhaust gas. This oxygen rate can be easily reached by using an exhaust gas analyser.

$$e_{\mathrm{air}} = \frac{P_{O_2}\left[\left[\left(x+\frac{y}{4}-\frac{z}{2}\right)\frac{\chi_{N_2}}{\chi_{O_2}}+x+\frac{y}{2}\right]+\frac{w}{(1-w)}\frac{M_{C_xH_yO_z}}{M_{H_2O}}\right]}{\left(x+\frac{y}{4}-\frac{z}{2}\right)\left[1-P_{O_2}\left(1+\frac{\chi_{N_2}}{\chi_{O_2}}\right)\right]} \tag{24}$$

The oxygen rate in the exhaust gas is controlled by the device by adjusting the fan speed. For the tested μCHP device, the oxygen rate in wet exhaust gas is equal on average to 6.2% for any PLR that leads to an air excess of 48%. The ash and exhaust gas mass flows are calculated by Eqs. (25) and (26). For the calculation of the exhaust gas mass flow, the ash mass flow is neglected.

$$\dot{m}_{\mathrm{ash}} = Y_{\mathrm{ash}}\,\dot{m}_{\mathrm{fuel}} \tag{25}$$

$$\dot{m}_{\mathrm{exh}} = \dot{m}_{\mathrm{fuel}} + \dot{m}_{\mathrm{air}} \tag{26}$$

The CO and the NO masses have been integrated during the transient phases in order to be used in the numerical model. For each starting cycle, an emission value for the CO and NO emissions is incremented like Persson et al. did for WP boilers and stoves [33]. Table 4 summarizes these values. During the steady state phase, the model takes into account the CO and the NO emissions by Eqs. (28) and (30). The gas analyser gives the CO and the NO volumetric content in the wet exhaust gas. Eq. (27) gives the volume flow of the exhaust gas and Eq. (29) gives the NO emission variation according to the PLR (Fig. 6).

$$\dot{V}_{\mathrm{exh}} = \dot{m}_{\mathrm{fuel}}V_m\left[\frac{w}{M_{H_2O}}+\frac{(1-w)}{M_{C_xH_yO_z}}\left[\frac{y}{2}+x+\left(e_{\mathrm{air}}+\frac{\chi_{N_2}}{\chi_{O_2}}(1+e_{\mathrm{air}})\right)\times\left(x+\frac{y}{4}-\frac{z}{2}\right)\right]\right] \tag{27}$$

$$\dot{m}_{CO} = \rho_{CO}\dot{V}_{\mathrm{exh}} \tag{28}$$

$$\rho_{NO} = f(\mathrm{PLR}-\mathrm{PLR}_{\mathrm{nom}}) + \rho_{NO}^{\mathrm{nom}} \tag{29}$$

$$\dot{m}_{NO} = \rho_{NO}\,\dot{V}_{exh} \tag{30}$$

4.4. Exhaust gas heat losses model

For the model, different temperatures are required: the fuel temperature, the combustion air temperature, exhaust gas temperature and ash temperature. The fuel and air temperature are

Table 4
Parameters of the model.

	Parameter	Value	Unit
Steady state parameters			
1	$\mathrm{PLR}_{\mathrm{nom}}$	100	%
2	$\dot{m}_{\mathrm{fuel}}^{\mathrm{nom}}$	3.894	kg/h
3	$\dot{Q}_{HX}^{\mathrm{nom}}$	16,559	W_{th}
4	$P_{\mathrm{gross}}^{\mathrm{nom}}$	1707	W_{el}
5	$P_{\mathrm{aux}}^{\mathrm{nom}}$	174	W_{el}
6	$T_{\mathrm{exh}}^{\mathrm{nom}}$	168	°C
7	e_{air}	0.47	–
8	a	0.03483	(kg/h)/100
9	b	152.18	W_{th}/100
10	c	16.31	W_{el}/100
11	d	0.784	W_{el}/100
12	e	0.605	°C/100
13	f	0.79	μg/(n)m^3/100
14	ρ_{CO}	36	μg/(n)m^3
15	ρ_{NO}^{nom}	178	μg/(n)m^3
Transient state parameters			
16	$\mathrm{PLR}_{\mathrm{start}}$	27	%
17	$\mathrm{PLR}_{\mathrm{stop}}$	0	%
18	$\mathrm{PLR}_{\mathrm{modu}}$	8	%
19	$\dot{Q}_{HX}$	6	W_{th}/s
20	$\dot{P}_{\mathrm{gross}}$	0.6	W_{el}/s
21	$\Delta t_{\mathrm{start}}^{Q}$	450	s
22	$\Delta t_{\mathrm{start}}^{P}$	670	s
23	$\Delta t_{\mathrm{stop}}^{Q}$	2000	s
24	$\Delta t_{\mathrm{stop}}^{P}$	200	s
25	$\tau_{\mathrm{start}}^{Q}$	30	s
26	$\tau_{\mathrm{start}}^{P}$	8	s
27	τ_{stop}^{Q}	800	s
28	k_{stop}^{P}	3	W_{el}/s
29	E_{start}^{P}	142	Wh_{el}
30	E_{stop}^{P}	38	Wh_{el}
31	mv_{CO}^{start}	3.4	kg/((n)m^3/s)
32	mv_{NO}^{start}	0.20	kg/((n)m^3/s)
33	mv_{CO}^{stop}	3.7	kg/((n)m^3/s)
34	mv_{NO}^{stop}	0.16	kg/((n)m^3/s)

defined freely by the user to constant or variable values. The exhaust gas temperature is assessed by a linear relation (Eq. (31)) depending on PLR.

$$T_{exh} = T_{exh}^{nom} + e(PLR - PLR_{nom}) \quad (31)$$

There are different energy flows created by the incoming and out coming components of the system. Here, these energy flows are called the enthalpy flows and they are linked to a temperature difference between the combustion reactants (fuel and air) and the combustion products (ash, CO_2, N_2, O_2 and CO). These enthalpy flows are calculated by using specific heats or directly specific enthalpies. To determine the enthalpy flows of the biomass fuel, Wenzl [34] gives an empirical formula of the specific heat of dry and wet biomass fuel:

$$c_{fuel} = \left(1114 + 4.86\,T_{fuel}\right)(1 - w) + 4180\,w \quad (32)$$

The enthalpy flow of the biomass fuel becomes:

$$\dot{H}_{fuel} = \dot{m}_{fuel}\,c_{fuel}\left(T_{fuel} - T_{ref}\right) \quad (33)$$

The enthalpy flow of the latent heat losses is calculated by using latent heat of water:

$$\dot{H}_{exh}^{lat} = \dot{m}_{H_2O} L_v \quad (34)$$

The exhaust heat losses linked to the others components are assessed by using the specific enthalpy of each combustion product. These specific enthalpies are extracted from JANAF tables [35] which give the specific enthalpy of each component i according to its temperature in K. The reference temperature is taken at 273 K.

$$\dot{H}_i = \frac{\dot{m}_i}{M_i}\left(H_i(T_i) - H_i\left(T_{ref}\right)\right) \quad (35)$$

The exhaust gas heat losses are not recovered here that's why this quantity is not included in the thermal production however the assessment of this quantity gives the possibility to integrate an additional system to recover this heat and to increase the efficiency of this system.

The heat losses by the skin of the μCHP device are worked out by Eq. (36). The values have been compared to basic heat losses calculations using a heat exchange coefficient and a temperature difference between the mean internal air temperature and the ambient temperature. By default, this quantity is not recovered by considering the device is not located in the heated space, but there is the possibility to use this value as internal gain in a building dynamic thermal simulation.

$$\dot{Q}_{loss} = \dot{H}_{fuel} + \dot{H}_{air} + P_{fuel} - P_{gross} - \dot{Q}_{HX} - \dot{H}_{exh} \quad (36)$$

Finally, the model has 34 parameters, 15 for the steady state characterization and 19 for the transient states characterization. Table 4 sums up all the 34 parameters with the values.

Table 5
Maximum deviations between the model and the experimental results in steady state.

PLR [%]	22	30	41	50	61	70	80	90	98
E_{fuel} [%]	−0.6	−1.2	0.9	0.1	−3.2	−3.2	−0.6	1.8	0.1
E_{th} [%]	−0.2	−0.6	−0.3	2.5	−3.6	−2.1	−0.2	2.6	1.0
E_{el} [%]	3.5	0.2	3.0	−2.7	−3.1	−3.6	−1.2	3.6	1.6
T_{exh} [%]	6.0	−3.3	−2.7	−1.5	1.0	−1.4	1.2	5.2	3.0

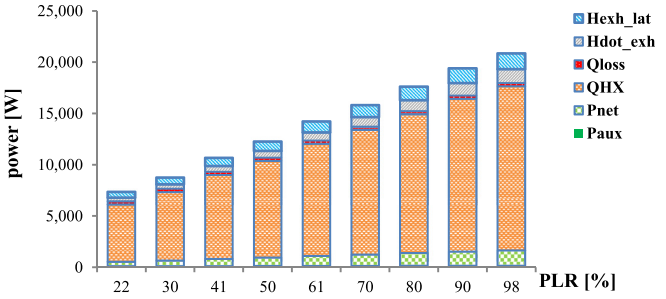

Fig. 11. Energy balance of the model of the WP μCHP device.

4.5. Validation of the model and discussion

The performances of the WP μCHP have been compared in steady states to the model. Maximum deviations of 3.2% has been found for the fuel energy, 3.6% for the thermal energy, 3.6% for the gross electrical energy and 6% for the exhaust gas temperature (Table 5). The minimum duration tests were 3 h.

The model has been compared to dynamic experimental tests which were not used to calibrate the model. The thermal and electrical energies produced on the whole cycle are compared to the model for 2 cases. Two characteristic test durations have been used: the minimum duration test to get good cycle electrical efficiencies (Fig. 12) and the maximum duration test in order to fully load the heat storage tank. The first case is a 3 h long test at 70% of PLR and the second is a 9 h long test at 70% of PLR. The model presents an acceptable accuracy with a maximum deviation of 5.3% for the electrical energy of the test 1 (Table 6).

The R-square value (determination coefficient) of each trend line for the steady and transient states is given on Figs. 3 and 4 and 6–9.

Fig. 11 shows the energy balance of the μCHP device for different PLR. The main heat losses are the exhaust gas heat losses. A heat recovery on exhaust gas by using a condensation boiler could improve the global efficiency of the system. The heat production is preponderant compared to the electrical production which is low that is mainly linked to the used technology (steam engine) and to the power scale. The heat losses are low that let to reach high efficiencies even at low PLR (Fig. 5).

The initial motivation is to provide a dynamic model to be suitable with annual dynamic thermal simulations for building energy simulations and to correctly model the behaviour of a WP μCHP to cover heat and power needs with power needs which can be very variable. Fig. 12 shows the ratio between the electrical efficiency of an operating cycle and the nominal electrical efficiency according to the cycle duration. This normalized efficiency takes into account that the electrical energy which is consumed during the start-up phase (starter, HP pump) has to be recovered during the beginning of the engine operation before considering that the electrical production supplies the building. The cycle should last at

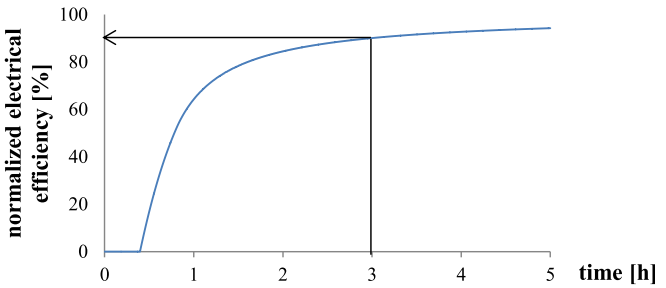

Fig. 12. Normalized electrical efficiency of a cycle according to the operating time of the cycle.

Table 6
Comparison between the model and experimental tests on 2 dynamic cycles.

	E^P_{exp}[kWh$_{el}$]	E^P_{model}[kWh$_{el}$]	Deviation [%]	E^Q_{exp}[kWh$_{th}$]	E^Q_{model}[kWh$_{th}$]	Deviation [%]
Test 1	2.66	2.80	5.3	31.32	32.60	4.1
Test 2	10.69	10.65	−0.4	109.93	107.10	−2.7

least 3 h to obtain interesting electrical efficiencies (90% of the nominal value, Fig. 12). The delay time before the engine triggering being at least 600 s, the modulation and a heat storage system appear as essential to take maximum advantage of these systems.

5. Conclusion

A WP μCHP device has been tested in order to know its energetic and environmental performances. Then a data driven model of a steam engine WP μCHP, based on previous experimental studies, has been developed and implemented in the TRNSYS numerical environment. Both the steady state and the transient phases are modelled according to the PLR. It has been shown that the inlet water temperature and the mass flow rate of the cooling water have an insignificant influence on the energetic and environmental performances of the device. Experimental investigations lead to an electrical efficiency of about 9% and a global efficiency of about 95% at full load. The PLR is the main parameter having a significant influence on the performances of the device. The electrical, thermal and global efficiencies are lower at the minimum PLR with an electrical efficiency of about 7.2% and a global efficiency of 88%. The pollutant emissions (CO, CO_2, NO and ash) have also been studied. The model just needs 34 experimentally reachable parameters to well characterize the steady state and the transient phases by assessing all the energy flows involved in the system and the pollutant emissions. The study of the transient phases highlights that the cycle durations have to be long to get high electrical efficiencies and low pollutant emissions impacts. The modelling of the transient phases will let to implement more realistic numerical studies in order to assess the relevance of these systems when they are coupled with buildings. This model will be used to carry out optimization studies in order to optimize the coupling between buildings and this kind of innovative device by considering energetic, economic and environment criteria. The main goal is to optimize both the power and the heat productions and improve the power self-consumption while ensuring the thermal comfort.

Acknowledgements

The authors would like to thank Region Alsace for the financial support given to the present study, the firm De Dietrich for the supplying of the storage tank and the EIFER institute for having carried out laboratory tests of our wood pellet samples.

Nomenclature

c	specific heat (J/kg/K)
E	energy (Wh)
e_{air}	air excess (−)
$\dot{H}$	enthalpy flux (W)
H	specific enthalpy (J/mol)
LHV	lower heating value (kWh/kg$_{fuel}$)
L_v	water latent heat (J/kg)
M	molar mass (kg/mol)
m	mass (g)
mv	mass to volume flow rate ratio (kg/((n)m^3/s)
$\dot{m}$	mass flow (kg/s)
P	power (W)
P'	power ramp rate (W/s)
P_{O_2}	oxygen volume rate (%)
PLR	part load ratio (%)
$\dot{Q}$	thermal power (W)
$\dot{Q}'$	thermal power ramp rate (W/s)
t	time (s)
T	temperature (°C or K)
V	volume (m^3 or m^3/kg)
$\dot{V}$	volume flow (m^3/s)
V_m	molar volume (m^3/(n)mol)
w	water content (kg$_{water}$/kg$_{fuel}$)
x	molar fraction of carbon (−)
Y	mass fraction (−)
y	molar fraction of hydrogen (−)
z	molar fraction of oxygen (−)

Greeks symbols

Δt	time (s)
η	efficiency (%)
ρ	density (kg/m^3 or μg/(n)m^3)
σ	power to heat ratio (−)
τ	time constant (s)
χ	volume fraction (−)

Subscripts and exponents

air	air
amb	ambiant
ash	ash
aux	auxiliary
cw	cooling water
dry	dry part of the biomass fuel
el	electrical
exh	exhaust gas
exp	experimental
fuel	fuel
g	global
gross	gross part of the electrical production
HX	heat exchanger
i	inlet
lat	latent
loss	losses
model	modelling
modu	modulation
net	net part of the electrical production
nom	nominal
o	outlet
P	electrical power
PV	process value
Q	thermal power
ref	reference
SP	set point
start	start phase
stop	stop phase
tank	tank
th	thermal

Appendix 1. Steady state to transient states transition conditions.

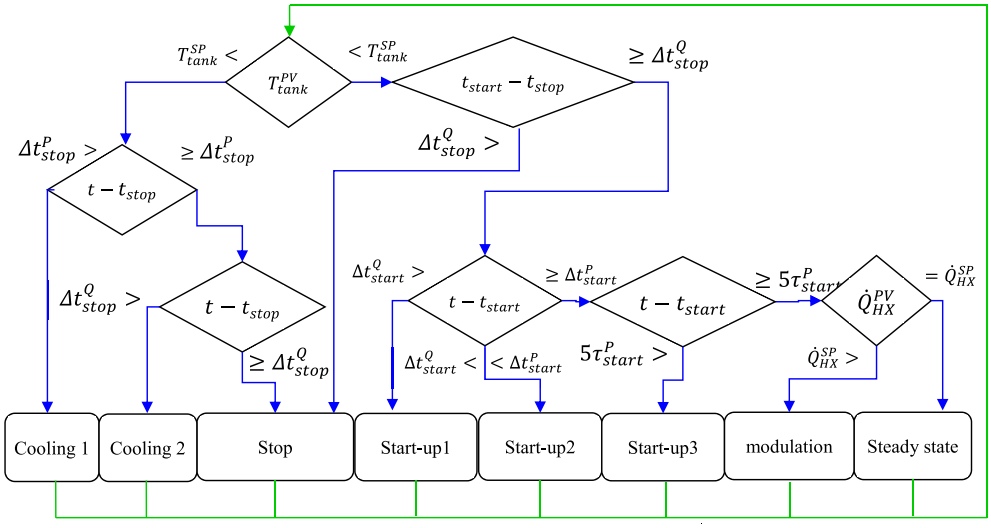

Current mode	Future mode	Trigger
Stop	Start-up1	$T_{tank}^{PV} < T_{tank}^{SP}$
Start-up1	Start-up2	End for $t - t_{start} > \Delta t_{start}^{Q}$
Start-up2	Start-up3	End for $t - t_{start} > \Delta t_{start}^{P}$
Start-up3	modulation	End for $t - t_{start} > 5\tau_{start}^{P}$
Modulation	Steady state	End for $\dot{Q}_{HX}^{PV} = \dot{Q}_{HX}^{SP}$
Steady state	Cooling 1	End for $t - t_{stop} > \Delta t_{stop}^{P}$
Cooling 1	Cooling 2	End for $t - t_{stop} > \Delta t_{stop}^{Q}$
Cooling 2	stop	End for $t_{start} - t_{stop} > \Delta t_{stop}^{Q}$

Appendix 2. Algorithm chart

- internal parameters surrounded in dotted orange line.
- 34 external parameters to be identified surrounded in solid orange line.
- main outputs surrounded in blue line.
- main inputs surrounded in black line.

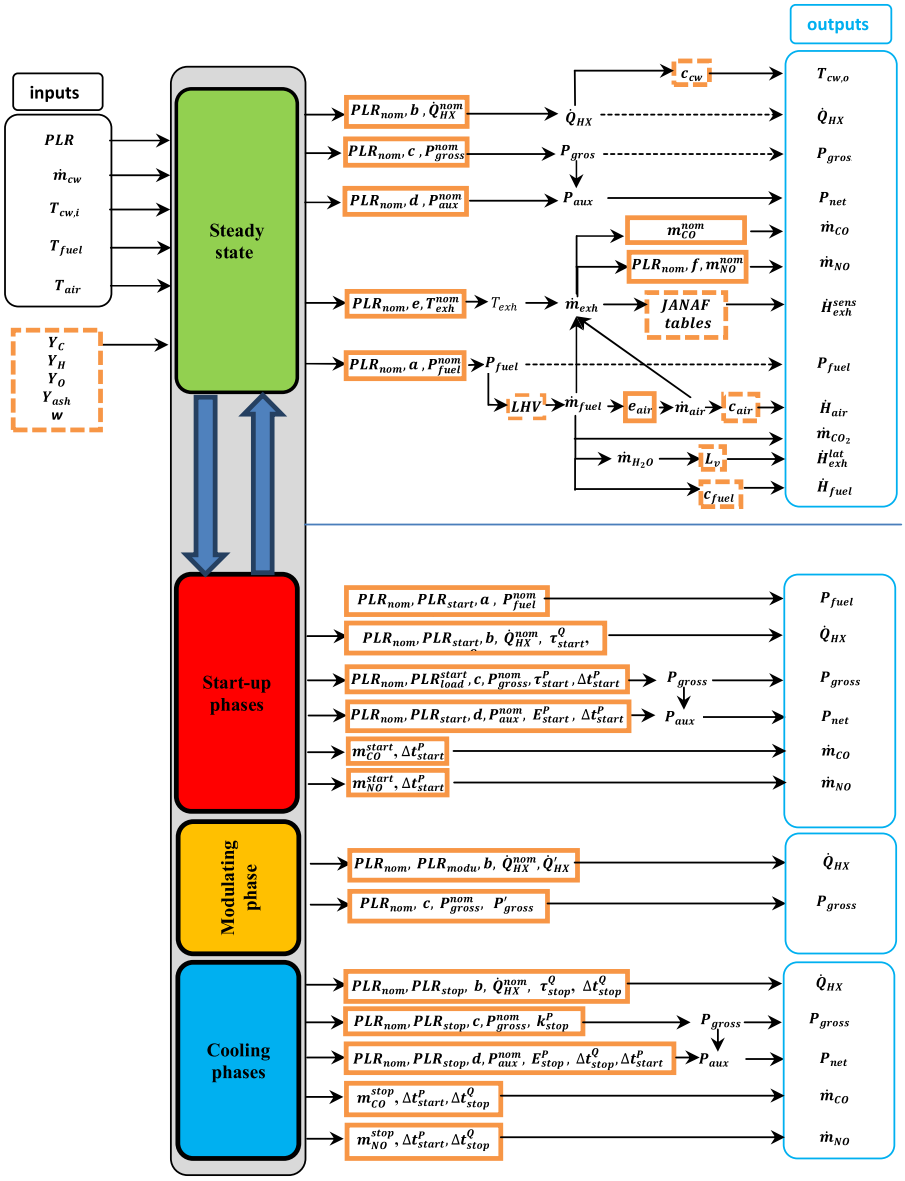

At first, according to the control strategy (heat led, power led), the PLR set point is calculated:

$$\mathrm{PLR_{SP}} = \frac{\dot{Q}_{\mathrm{HX}}^{\mathrm{SP}} - \dot{Q}_{\mathrm{HX}}^{\mathrm{nom}}}{b} + \mathrm{PLR_{nom}}$$

$$\mathrm{PLR_{SP}} = \frac{P_{\mathrm{gross}}^{\mathrm{SP}} - P_{\mathrm{gross}}^{\mathrm{nom}}}{c} + \mathrm{PLR_{nom}}$$

Appendix 3. Modelling representation of the start-up phase and the cooling phase.

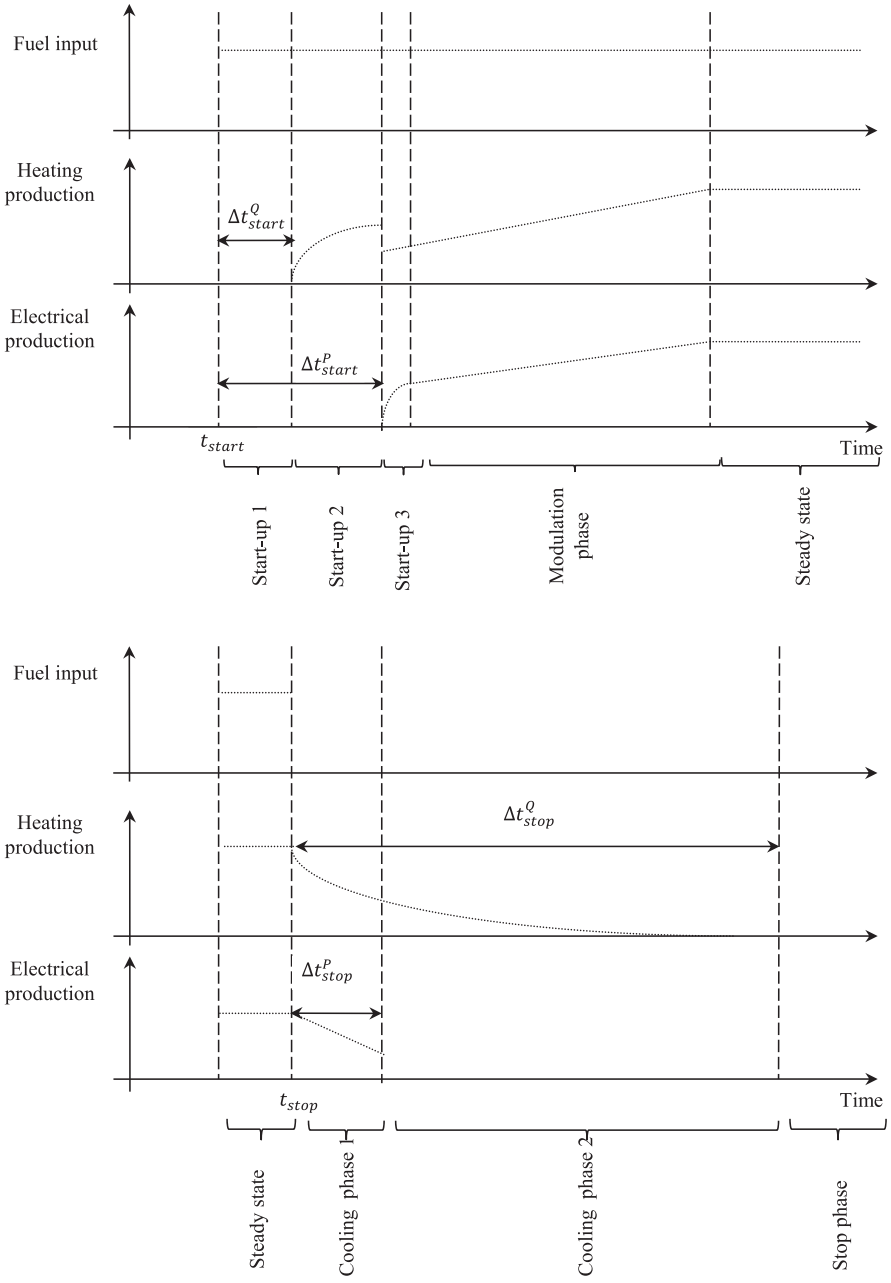

References

[1] Michele Bianchi, Andrea De Pascale, Pier Ruggero Spina, Guidelines for residential micro-CHP systems design, Appl. Energy 97 (September 2012) 673–685.

[2] Giovanni Angrisani, Michele Canelli, Antonio Rosato, Carlo Roselli, Maurizio Sasso, Sergio Sibilio, Load sharing with a local thermal network fed by a micro cogenerator: thermo-economic optimization by means of dynamic simulations, Appl. Therm. Eng. 71 (2014) 628–635.

[3] Pedro Gonçalves, Giovanni Angrisani, Carlo Roselli, Adélio R. Gaspar, Manuel Gameiro da Silva, Comparative energy and exergy performance assessments of a microcogenerator unit in different electricity mix scenarios, Energy Convers. Manag. 73 (September 2013) 195–206.

[4] The European Association for the Promotion of Cogeneration, European Project EDUCOGEN, a Guide to Cogeneration, Belgium, Brussels, March 2001.

[5] Benoît Andlauer, Systemic Optimization of Micro CHP Devices Integrated to Buildings (Optimisation systémique de micro-cogénérateurs intégrés aux bâtiments), Ph.D. Thesis, Mines ParisTech, Paris, France, 2011.

[6] Tekena Craig Fubara, Franjo Cecelja, Aidong Yang, Modelling and selection of micro-CHP systems for domestic energy supply: the dimension of network-wide primary energy consumption, Appl. Energy 114 (February 2014) 327–334.

[7] H.I. Onovwiona, V.I. Ugursal, Residential cogeneration systems: review of the current technology, Renew. Sustain. Energy Rev. 10 (5) (October 2006) 389–431.

[8] Kari Alanne, Kari Saari, Maunu Kuosa, Juha Jokisalo, Andrew R. Martin, Thermo-economic analysis of a micro-cogeneration system based on a rotary steam engine (RSE), Appl. Therm. Eng. 44 (November 2012) 11–20.

[9] Leilei Dong, Hao Liu, Saffa Riffat, Development of small-scale and micro-scale biomass-fuelled CHP systems – a literature review, Appl. Therm. Eng. 29 (11–12) (August 2009) 2119–2126.

[10] Stéphane Thiers, Bernard Aoun, Bruno Peuportier, Experimental characterization, modeling and simulation of a wood pellet micro-combined heat and power unit used as a heat source for a residential building, Energy Build. 42 (6) (June 2010) 896–903.

[11] Evelyn Cardozo, Catharina Erlich, Anders Malmquist, Lucio Alejo, Integration of a wood pellet burner and a stirling engine to produce residential heat and power, Appl. Therm. Eng. 73 (2014) 671–680.

[12] Guoquan Qiu, Yingjuan Shao, Jinxing Li, Hao Liu, Saffa Riffat, Experimental investigation of a biomass-fired ORC-based micro-CHP for domestic applications, Fuel 96 (June 2012) 374–382.

[13] Stefano Cordiner, Vincenzo Mulone, Experimental–numerical analysis of a biomass fueled microgeneration power-plant based on microturbine, Appl. Therm. Eng. 71 (2014) 905–912.

[14] Kari Alanne, Timo Laukkanen, Kari Saari, Juha Jokisalo, Analysis of a wooden pellet-fueled domestic thermoelectric cogeneration system, Appl. Therm. Eng. 63 (1) (February 2014) 1–10.

[15] M. Creyx, E. Delacourt, C. Morin, B. Desmet, P. Peultier, Energetic optimization of the performances of a hot air engine for micro-CHP systems working with a Joule or an Ericsson cycle, Energy 49 (January 2013) 229–239.

[16] Dario Prando, Francesco Patuzzi, Giovanni Pernigotto, Andrea Gasparella, Marco Baratieri, Biomass gasification systems for residential application: an integrated simulation approach, Appl. Therm. Eng. 71 (1) (October 2014) 152–160.

[17] G. Angrisani, K. Bizon, R. Chirone, G. Continillo, G. Fusco, S. Lombardi, F.S. Marra, F. Miccio, C. Roselli, M. Sasso, R. Solimene, F. Tariello, M. Urciuolo, Development of a new concept solar-biomass cogeneration system, Energy Convers. Manag. 75 (November 2013) 552–560.

[18] Frederic Lontsi, Oumarou Hamandjoda, Kennedy Fozao, Pascal Stouffs, Jean Nganhou, Dynamic simulation of a small modified Joule cycle reciprocating Ericsson engine for micro-cogeneration systems, Energy 63 (December 2013) 309–316.

[19] I. Beausoleil-Morrison, N. Kelly, Specifications for Modelling Fuel Cell and Combustion-based Residential Cogeneration Device within Whole-building Simulation Programs, IEA/ECBCS Annex 42 Subtask B Report, Natural Resources Canada, Canada, 2007.

[20] K. Lombardi, V.I. Ugursal, I. Beausoleil-Morrison, Proposed improvements to a model for characterizing the electrical and thermal energy performance of stirling engine micro-cogeneration devices based upon experimental observations, Appl. Energy 87 (10) (October 2010) 3271–3282.

[21] G. Conroy, A. Duffy, L.M. Ayompe, Validated dynamic energy model for a stirling engine μ-CHP unit using field trial data from a domestic dwelling, Energy Build. 62 (July 2013) 18–26.

[22] Elmar Pohl, David Diarra, A method to determine primary energy savings of CHP plants considering plant-side and demand-side characteristics, Appl. Energy 113 (January 2014) 287–293.

[23] L. Spitalny, J.M.A. Myrzik, T. Mehlhorn, Estimation of the economic addressable market of micro-CHP and heat pumps based on the status of the residential building sector in Germany, Appl. Therm. Eng. 71 (2014) 838–846.

[24] Adam Hawkes, Matthew Leach, Impacts of temporal precision in optimisation modelling of micro-combined heat and power, Energy 30 (10) (July 2005) 1759–1779.

[25] R.-J. Moffat, Describing the uncertainties in experimental results, Exp. Therm. Fluid Sci. 1 (1988) 3–17.

[26] AFNOR, Guide for the Expression of Uncertainty in Measurement (Guide pour l'expression de l'incertitude de mesure), Norme NF ENV 13005 (X07–020), 1999.

[27] M. Priel, Measurement uncertainties and tolerances (Incertitudes de mesure et tolérances), Tech. l'ingénieur R 285 (1999). France.

[28] B.N. Taylor, C.E. Kuyatt, Guidelines for Evaluating and Expressing the Uncertainty of NIST Measurement Results, NIST, Gaithersburg, USA, 1994. Technical Note 1297.

[29] J.-P. Holman, Heat Transfer, Mac Graw Hill, New York, USA, 1986.

[30] Claude Bernard, Characterization and Optimization of the Combustion of Wood in Fragmented Automatic Boiler (Caractérisation et Optimisation de la Combustion de Bois Fragmenté en Chaufferies Automatiques), Ph.D Thesis, University Henri Poincaré of Nancy I, Nancy, France, 2005.

[31] Amadeo Rossi, Fuel characteristics of wood and nonwood biomass fuels, Prog. Biomass Convers. 5 (1984) 69–99.

[32] EN 14961-2, Solid Biofuels – Fuel Specification and Classes – Part 2: Wood Pellets for Non-industrial Use, 2012.

[33] Tomas Persson, Frank Fiedler, Svante Nordlander, Chris Bales, Janne Paavilainen, Validation of a dynamic model for wood pellet boilers and stoves, Appl. Energy 86 (5) (May 2009) 645–656.

[34] H. Wenzl, The Chemical Technology of Wood, Academic Press, New York, USA, 1970.

[35] Chase, M.-W., NIST JANAF Thermochemical Tables, Journal of Physical and Chemical Reference, American Institute of Physic, Woodbury, USA, 1998.